Supplementary Materials for Security Risks of VOA-Induced Luminescence in Chip-Based Quantum Key Distribution

Zijian Li[a], Chenyu Xu[a], Xin Hua[b,c], Yongqiang Du[a], Xin Liu[a], Tao Lin[a], Xi Xiao[b,c], Kejin Wei[a]

[a] *Guangxi Key Laboratory for Relativistic Astrophysics, School of Physical Science and Technology, Guangxi University, Nanning 530004, China.*
[b] *National Information Optoelectronics Innovation Center (NOEIC), Wuhan 430074, China.*
[c] *State Key Laboratory of Optical Communication Technologies and Networks, China Information and Communication Technologies Group Corporation (CICT), 430074 Wuhan, China*

1. Experimental details and data for verification of parasitic EL

This section provides supplementary experimental details supporting the verification of parasitic electroluminescence (EL). It includes the specific procedures for confirming that the VOA exhibits *p–n* junction behavior and representative raw data from the luminescence tests.

1.1. Verification of the p–n junction structure

To elucidate the physical origin of the parasitic EL observed in the VOA, we experimentally verify whether the device incorporates an intrinsic *p–n* junction. The presence of such a junction is a prerequisite for carrier injection and radiative recombination under forward bias. A standard and unambiguous diagnostic is provided by the current–voltage (*I–V*) characteristic, as a *p–n* junction exhibits a distinct nonlinear response governed by diode transport physics.

According to the Shockley diode model, the forward-bias current of an ideal *p–n* junction follows an exponential dependence on the applied voltage,

$$I \propto \exp\left(\frac{qV}{\beta kT}\right), \tag{S1}$$

where q is the elementary charge, k is the Boltzmann constant, T is the absolute temperature, and β is the ideality factor. The parameter β captures the dominant carrier transport mechanism and typically varies with bias voltage in practical devices.

Figure S1 shows the measured forward-bias *I–V* characteristic of the VOA plotted on a semi-logarithmic scale. The data exhibit multiple quasi-linear regions, indicating exponential current-voltage relations with different effective ideality factors. Such behavior is a hallmark of *p–n* junction transport and reflects transitions between distinct conduction regimes as the bias increases.

At low forward bias, carrier injection is weak and the current is dominated by recombination processes within the space-charge region, leading to an ideality factor close to $\beta \approx 2$. With increasing bias, diffusion current becomes dominant and the ideality factor approaches the diffusion-limited value $\beta \approx 1$. At still higher bias, high-level injection effects emerge, causing the ideality factor to increase again toward $\beta \approx 2$. Finally, at sufficiently large voltages, series resistance limits the current, and the *I–V* curve deviates from exponential behavior.

To quantitatively extract the ideality factor, we analyze the slope of the semi-logarithmic *I–V* curve following the method of Ref. [1]. Writing the Shockley relation in base-10 logarithmic form,

$$\log_{10}(I) = \frac{q \log_{10}(e)}{\beta kT} V, \tag{S2}$$

the slope $S = d\log_{10}(I)/dV$ is given by

$$S = \frac{q \log_{10}(e)}{\beta kT}. \tag{S3}$$

The ideality factor can therefore be expressed as

$$\beta = \frac{q \log_{10}(e)}{S\,kT} \approx \frac{q}{2.3\,S\,kT}, \tag{S4}$$

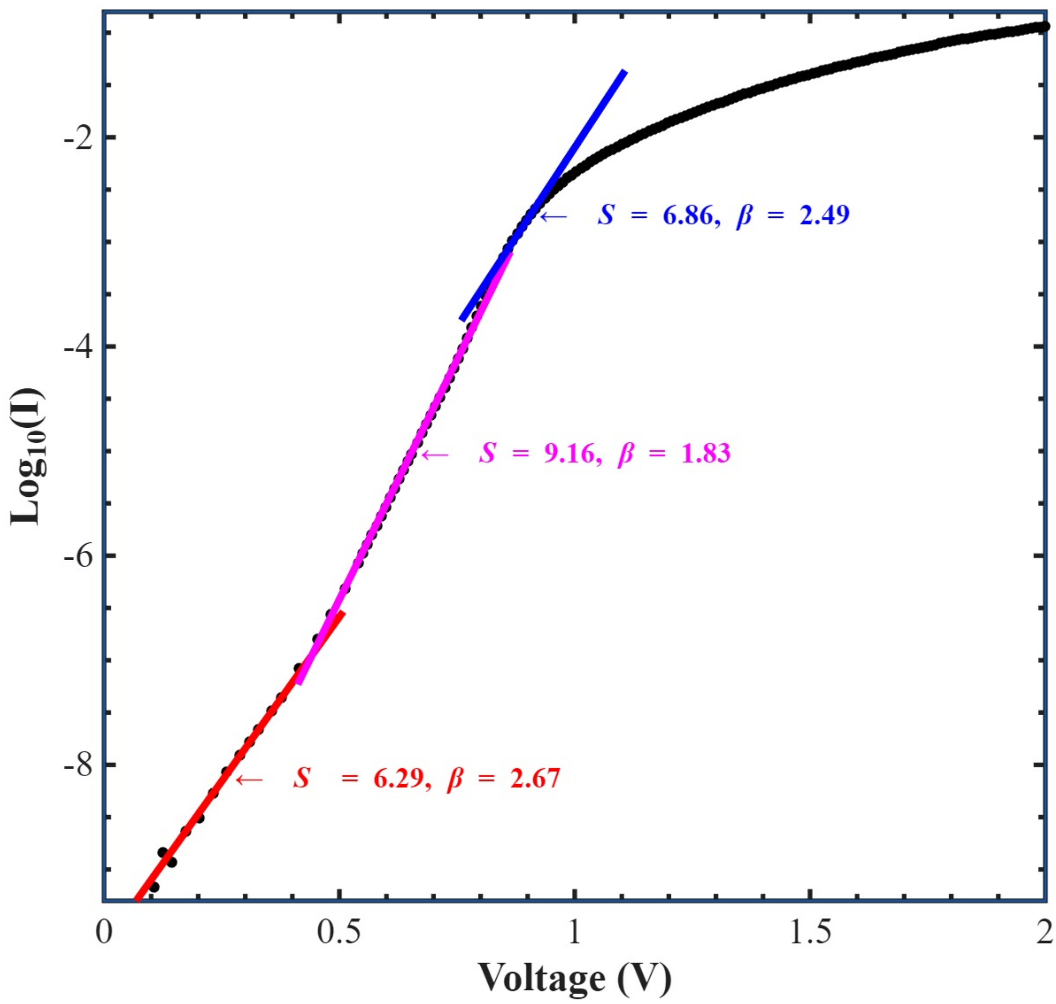

Figure S1: Semi-logarithmic current-voltage characteristics of the VOA under forward bias. The current is plotted on a logarithmic scale, whereas the voltage is plotted on a linear scale. Black filled circles represent the experimental data. The red, magenta, and blue solid lines indicate linear fits in three bias regions: 0-0.45 V, 0.50-0.80 V, and 0.85-0.90 V, respectively. The extracted slopes are used to calculate the ideality factor *n* in each bias regime.

where the numerical factor arises from the conversion between natural and base-10 logarithms.

By performing linear fits on the data within the three bias regions indicated in Figure S1, we extract the corresponding slopes and ideality factors. In the low-bias region (0–0.45 V), the extracted value $\beta \approx 2.6$ is consistent with recombination-dominated transport. In the intermediate-bias region (0.50–0.80 V), β decreases to approximately 1.8, approaching the diffusion-limited regime. At higher bias (0.85–0.90 V), β increases again to ~ 2.5, signaling the onset of high-level injection. Beyond 0.90 V, the curve progressively deviates from exponential behavior, indicating the influence of series resistance.

Although the extracted ideality factors deviate slightly from their ideal integer values, such deviations are expected in practical integrated devices due to effects including contact resistance and material inhomogeneity. Importantly, the observed evolution of β with bias—from recombination-dominated to diffusion-dominated and back to high-injection behavior—constitutes a clear and internally consistent signature of a *p*–*n* junction. This provides direct experimental confirmation that the VOA incorporates an active *p*–*n* junction capable of supporting electrically driven EL.

1.2. Characterization of a 318-μm-long VOA fabricated by AMF

To demonstrate that VOA-induced luminescence is a general phenomenon independent of specific fabrication platforms, we characterized an additional 318 µm-long VOA fabricated on the AMF platform, in contrast to the CompoundTek-fabricated device used in the main text. Following the same experimental procedure as described in the main text, the forward-bias voltage was swept from 0 V to 2 V in steps of 0.1 V. The characterization results are presented in Figure S2. Notably, this device exhibits a turn-on voltage consistent with the observations in the main text and shows a similar voltage-dependent trend. Furthermore, owing to its increased length, the VOA displays an optical attenuation of 8.4 dB.

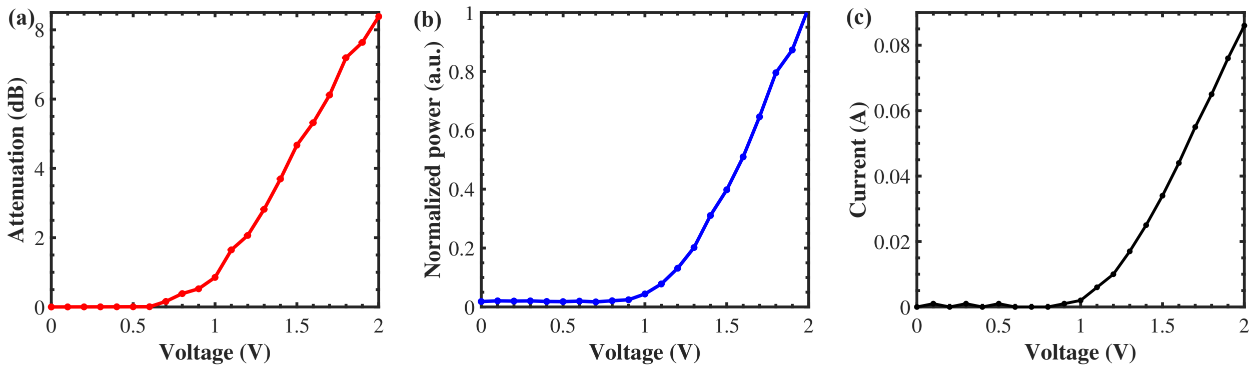

Figure S2: Characterization of the 318-μm-long VOA fabricated by AMF. (a) Measured optical attenuation, (b) normalized emitted power, and (c) current of the VOA as a function of the applied voltage. The filled circles represent the measured data, and the solid lines are guides to the eye connecting the data points.

1.3. Detailed experimental data for luminescence characterization

Detailed raw data and calibration parameters supporting the luminescence characterization presented in Fig. 3(b) of the main text are provided below. The data processing procedures are detailed in the Methods section of the main text.

Table S1 summarizes the raw photon count rates (c_i) measured at each applied (VOA) voltage, the corresponding calibrated detection efficiencies (η_i) for the four single-photon detectors (SPD$_i$, $i = 1, \ldots, 4$), and the corresponding VOA attenuation values. Here, Voltage denotes the driving voltage applied to the VOA. As shown in Table S1, the detection efficiency varies with this voltage. This variation occurs because a higher VOA voltage induces stronger luminescence, increasing the incident photon count rate. Since the detection efficiency of the single-photon detector depends on the incident photon count rate, it changes accordingly across different voltage settings. Table S2 lists the measured dark count rates (d_i) for each SPD. Finally, the calculated total corrected count rates (C_{correct}) for each measurement point, prior to normalization, are presented in Table S3.

Table S1: Calibrated detection efficiencies (η_i), the corresponding raw photon count rates (c_i) of the four SPDs, and the applied attenuation values at various voltage settings. The data presented in this table correspond to the measurements shown in Fig. 3 of the main text.

	SPD_1		SPD_2		SPD_3		SPD_4		
Voltage (V)	c_1 (cps)	η_1	c_2 (cps)	η_2	c_3 (cps)	η_3	c_4 (cps)	η_4	Attenuation (dB)
0.0	463	10.0%	464	10.0%	476	10.0%	459	10.0%	0.000
0.2	486	10.0%	462	10.0%	457	10.0%	408	10.0%	0.012
0.4	522	10.0%	464	10.0%	493	10.0%	474	10.0%	0.019
0.6	471	10.0%	467	10.0%	475	10.0%	478	10.0%	0.046
0.8	742	10.0%	910	10.0%	788	10.0%	749	10.0%	0.064
1.0	43325	10.0%	71433	10.0%	50939	10.0%	40206	10.0%	0.703
1.2	218229	9.0%	326650	7.9%	249973	8.1%	203120	9.0%	2.385
1.4	394528	7.6%	551664	6.9%	446032	7.4%	365960	7.9%	3.716
1.6	528394	6.9%	702993	6.2%	590240	6.6%	488041	7.0%	4.433
1.8	627376	6.5%	806390	5.7%	695721	6.2%	576818	6.6%	4.819
2.0	701710	6.2%	880519	5.3%	775279	6.0%	642187	6.5%	4.932

Table S2: Measured dark count rates (d_i) of the four single-photon detectors (SPD_i).

Detector (i)	Dark count rate, d_i (cps)
SPD_1	463
SPD_2	464
SPD_3	476
SPD_4	459

Table S3: Total corrected luminescence count rate C_{correct} versus the VOA driving voltage U.

U (V)	0	0.2	0.4	0.6	0.8	1.0	1.2	1.4	1.6	1.8	2.0
C_{correct} (cps)	18063	18075	19470	18852	31793	2052797	11877013	23859292	34984353	43852957	50829038

References

[1] Seiferth, F. Light emission from silicon (1994). Book.